

HandSeg: A Dataset for Hand Segmentation from Depth Images

Sri Raghu Malireddi*

Franziska Mueller†

Markus Oberweger‡

Abhishake Kumar Bojja*

Vincent Lepetit‡

Christian Theobalt†

Andrea Tagliasacchi*

*-University of Victoria, †-MPI Informatics, ‡-TU Graz

{raghu, abojja, ataiya}@uvic.ca

{frmueeller, theobalt}@mpi-inf.mpg.de

{oberweger, lepetit}@icg.tugraz.at

Abstract

We introduce a large-scale RGBD hand segmentation dataset, with detailed and automatically generated high-quality ground-truth annotations. Existing real-world datasets are limited in quantity due to the difficulty in manually annotating ground-truth labels. By leveraging a pair of brightly colored gloves and an RGBD camera, we propose an acquisition pipeline that eases the task of annotating very large datasets with minimal human intervention. We then quantify the importance of a large annotated dataset in this domain, and compare the performance of existing datasets in the training of deep-learning architectures. Finally, we propose a novel architecture employing strided convolution/deconvolutions in place of max-pooling and unpooling layers. Our variant outperforms baseline architectures while remaining computationally efficient at inference time. Source and datasets will be made publicly available.

1. Introduction

In everyday life we interact with the surrounding environment employing our hands as our analog controllers. As we would like to transfer this natural way of interaction to virtual environments, the development of robust hand tracking technology becomes a key requirement for the success of immersive AR/VR experiences. Thanks to depth cameras, substantial progress towards this goal has been made, where the state of the art involves a mixture of *generative* and *discriminative* methods to fulfill the objectives of efficiently/accurately tracking hand poses, and re-initializing properly in case of tracking failures. Most real-time tracking algorithms rely on the identification of the hand location in the image: generative trackers first need to identify the subset of the point cloud to which the digital model should be aligned; analogously, discriminative trackers assume the input of the regressor to be a rectangular region of fixed size,

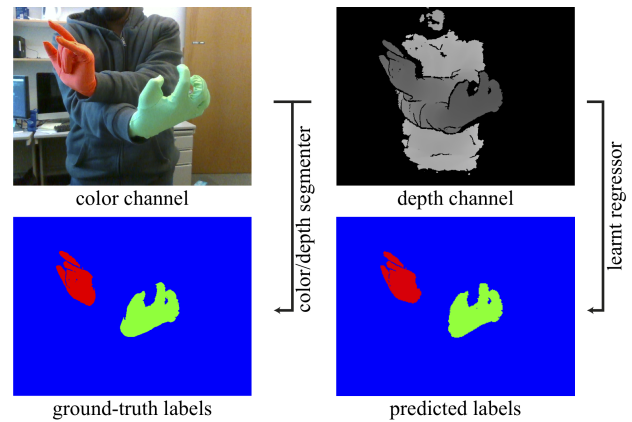


Figure 1. Our dataset is created by having a number of subjects performing in front of the camera while wearing a pair of colored gloves. Color and depth are then jointly exploited to automatically compute a ground-truth labeling without any user intervention. The mapping between input depth and ground truth labels is then exploited to learn a hand segmentation network for depth input.

with the hand roughly centered therein. Rather than tackling the generic problem of hand tracking, we focus our attention to the problem of *hand segmentation*, as robust solutions to this first step are essential to enable robust tracking.

A number of heuristic solutions have been proposed to simplify the task of hand segmentation [24, 18, 23, 37, 30]. While these approaches are well suited for small-scale lab experiments, they do not possess the robustness required for a consumer-level solution that needs to work under the full diversity of interaction in general real-world scenes: the violation of one of their underlying assumptions results in immediate tracking failure. One could learn a hand segmenter from a dataset of annotated depth images. However, as we will show, the limited size and quality of currently available datasets results in regressors that typically overfit to the training data, and do not generalize well to unseen scenarios. Further, in contrast to marker-based hand tracking,

and primarily due to the limited size of available datasets, the application of modern deep learning solutions to the problem of real-time hand segmentation has received limited attention. Hence, a central challenge is to capture a sufficiently *large* dataset equipped with *high-quality* ground truth annotations.

Our **first contribution** is the introduction of a new annotated dataset for hand segmentation from depth data. We obtain this dataset by having a number of users perform hand gestures in front of an RGBD camera while wearing a pair of *colored gloves*; see Figure 1. The color and depth channels are then used to generate high-quality ground truth annotations with minimal user intervention. This process allowed us to generate a high-quality annotated dataset that is two orders of magnitude larger than what is available in the literature¹. Our **second contribution** is the analysis of the use of this dataset towards the training of a segmenter that is appropriate for real-time hand tracking applications. We evaluate popular machine learning techniques for multi-class segmentation, and we propose a new convolutional neural network leveraging *strided [transposed-]convolutions* in place of [un]pooling layers. This allows the network to achieve high-accuracy (97.2% mean IoU), and a forward-propagation performance suitable to real-time applications ($\approx 5ms$ on an NVIDIA GTX980).

2. Related Work

We now introduce several heuristics that have been proposed for real-time hand segmentation, describe existing datasets, and overview techniques for semantic segmentation. For references on hand tracking, see [41].

2.1. Heuristics for hand segmentation

The pioneering approach of Oikonomidis et al. [24] leverages skin color segmentation and requires the user to wear long sleeves and to keep their face out of sight. Melax et al. [18] exploited short-range depth sensors by assuming that everything within the camera field of view is to be tracked, while Oberweger et al. [23] expect the hand to be the closest object to the camera. Some methods identify the ROI as the portion of the point cloud attached to the wrist, where this can be identified either with the help of a colored wristband [37], or by querying the wrist position in a full-body tracker [30]. As discussed, these heuristics stop working as soon as their underlying assumptions are violated.

2.2. Datasets for hand segmentation

Datasets for hand segmentation from color images were previously proposed by Buehler et al. [3] and Bambach et al.

¹Note how although [39] represents an exception to this statement, their annotations are generated via heuristics starting from input fingertip annotations. In our evaluation we clearly demonstrate how these annotations result in a significant loss of learning performance.

[2] who provided pixel-level manually annotated ground truth for respectively ≈ 500 and $\approx 15k$ color images. Manual annotation of segmentation masks from color images is extremely labor intensive. This not only makes it very difficult to collect large-scale datasets, but the quality of annotations also depends on the skills of individual annotator. Gathering bounding-box annotations is easier, as demonstrated by the datasets of ≈ 500 annotated images in Everingham et al. [6], the $\approx 5k$ images in [14], or the $\approx 15k$ images in Mittal et al. [19]. However, these annotations are too coarse for applications that require accurate hand/background or hand/object segmentation.

Automatic segmentation. Hand segmentation can be cast as a skin color segmentation problem [45]. However, segmenting this not only detects hands but also other skin regions, such as faces or forearms when the user is not wearing sleeves. Further, datasets of this kind [5, 44, 9] contain at most a few thousand manual annotations, which is magnitudes smaller than what is needed to train deep neural networks. Zimmermann and Brox [45] recently proposed a dataset of $\approx 44k$ *synthetic* images. However, it is notoriously difficult to accurately model skin colors and complex effects like subsurface scattering, making it challenging to develop segmentation methods that could work in the wild. Conversely, hand segmentation from *depth* images does not suffer this problem. Tompson et al. [38] pioneered this approach and painted each user hand with bright colors which are segmented and post-processed with the help of depth information. However, while [38] contains $\approx 70k$ marker-annotated frames from three viewpoints, only $\approx 7k$ are provided with annotations suitable for hand segmentation.

Segmentation via tracking. Recent datasets targeting hands have mostly focused on acquiring annotated 3D marker locations for joints [41]. Creating datasets via manual annotation is not only labor-intensive [34], but placing markers within a noisy depth map often results in inaccurate labels. Assuming marker locations are correct, simple heuristics can be employed to infer a dense labeling. Following this idea, Wetzler et al. [39] first employ a complex/invasive hardware setup comprising of magnetic sensors attached to fingertips to acquire their locations, and obtain the segmentation mask via a simple depth-based flood-fill algorithm. While the dataset in [39] contains $\approx 200k$ annotated exemplars, these heuristic annotations should not be considered to be ground truth for learning a high-performance segmenter; see our evaluations in Section 6.

2.3. Semantic segmentation

Recently, neural networks have been successfully applied to the problem of semantic segmentation of a broad range of real world objects and scenes. Popular methods include fully convolutional neural networks [17], encoding the input to a low-dimensional latent space, and decoding via

Dataset	Annotation	# Frames	# Subjects	Viewpoint	Hand?	Sensor Type	Resolution
HandSeg (Ours)	automatic	265,000	14	exo	left/right	RealSense SR300	640 × 480
Freiburg [45]	synthetic	43,986	20	exo	left/right	Synthetic Render	320 × 320
NYU [38]	automatic	6,736	2	exo	left	Microsoft Kinect v1	640 × 480
HandNet [39]	heuristic	212,928	10	exo	left	RealSense SR300	320 × 240

Table 1. A summary of datasets for hand segmentation from depth imagery.

bilinear upsampling to predict the semantic segmentation. Follow-up works perform learning at the decoder level as well, such as the well known architectures *DeconvNet* [22] and *SegNet* [1]; see Section 5. Learnt encoder-decoder architectures have been shown to perform well on semantic segmentation [42, 15, 27, 25], but when fast inference time is essential, random forests are an excellent alternative due to their easy parallelization [12, 31]. In human pose estimation applications, Shotton et al. [33] inferred body parts labels via random forests, which was later adopted for hand localization from depth images by Tompson et al. [38], and color images by Zimmermann and Brox [45]. In multi-view setups, effective segmentation provides a strong cue for effective tracking [16], and the two tasks can even be coupled into a single optimization problem [10]. Predicted segmentation masks can be noisy and/or coarse, and post-processing is typically employed to remove outliers by regularizing the segmentation [13, 4, 43]. A recent approach by Kolkin et al. [11] accounts for the severity of mis-labeling by a loss encoding their spatial distribution, but this method has yet to be generalized to a multi-label classification scenario like ours. Relevant to our work is also the recent R-CNN series of works, of which the instance segmentation work by He et al. [7] represents the latest instalment. While combining bounding box localization with dense segmentation could be effective, it is however unclear to which extent such networks could be adapted to demanding real-time applications such as hand tracking.

3. Overview

Compared to manual annotation, the synchronized color/depth input of an RGBD device can be exploited to generate automatic annotations of hand segmentations at a larger scale. As we attempt to regress a labeling from depth images only, the color channel of RGBD images can be used to (quasi) non-invasively instrument our acquisition. More specifically, we record subjects performing hand motions in front of a depth camera while wearing *skin-tight* gloves; see Figure 2. As the gloves fit the user’s hand tightly, minimal geometric aberration to the depth map occurs, while the consistent color of the glove can be used to extract the hand ROI via a joint color/depth-based segmentation; see Section 4. In this process, the *only* interaction required is to *discard* the few images that have been incorrectly segmented. In



Figure 2. Our dataset is constructed by recording a user performing hand movements wearing a pair of bright colored gloves in front of a depth camera. To the best of our knowledge, our dataset is the first *two-hand* dataset for hand segmentation.

Section 5, we overview well-known learning approaches to semantic segmentation, and propose a novel hybrid network architecture. The performance of the dataset, as well as the one of the newly proposed network is evaluated against the state of the art in Section 6.

4. Dataset acquisition

After an initial color calibration session, we acquire our dataset following a three-step process: we ask the user to perform a few motions according to the *protocol* described below while wearing a pair of colored gloves, and record sequences of (depth,color) image pairs at a constant 48Hz rate with an Intel RealSense SR300; we then execute a joint color/depth segmentation to generate masks with a very small false-positive rate; we finally quickly discard images containing erroneous labels via manual inspection. This task is significantly simpler than manually editing individual images. In our experiments, 20% of the automatically labeled images were discarded. The sequences we acquired are in exo-centric configuration, with one or two hands of subjects in the 20-50 age range; see Table 1 and Figure 2.

Color glove calibration. To simplify the task of color segmentation, the lighting conditions during acquisition are kept constant, and the camera is not moving. As shown in Figure 1, the gloves have a Lambertian material with a constant albedo, and a very weak specular component. This simplifies the calibration process, as the color of a pixel on the glove can be largely explained by the relative orientation of surface normal and light, with only minor brightness vari-

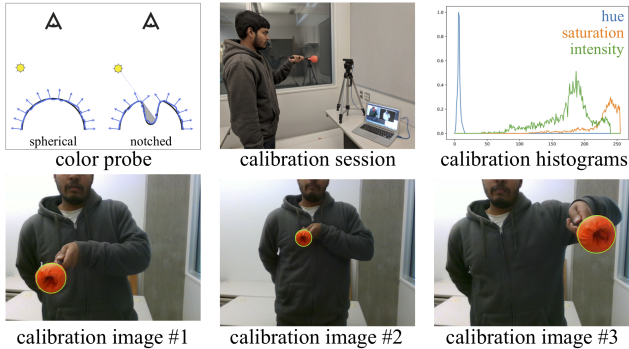


Figure 3. Our color calibration setup. (top-left) A hemisphere wrapped in the glove’s material contains all of the potential surface normals visible from the camera’s point of view. By notching the sphere, we also obtain color variations caused by ambient occlusion and self-shadowing. (top-middle) We calibrate the system by probing various parts of the view frustum, generating a set of calibration images (bottom). All the pixels within the detected circles participate in the computation of the color space (top-right).

ations caused by self-occlusions/shadows. To calibrate the gloves we then use a simple yet effective solution. As shown in Figure 3, we wrap the glove onto a sphere, and acquire calibration images by sparsely sampling the field of view with our probe. Due to its simple geometry and consistent color, the probe can be easily located, and all pixels within its circular profile are then used for color calibration. Similarly to what is commonly done for skin segmentation [26], we then convert the calibration images to HSV space, from where conservative min/max thresholds for every channel are then extracted.

Acquisition protocol. Similarly to Yuan et al. [41], we attempt to maximize the coverage of the articulation space by asking each user to assume a number of example extremal poses, while capturing the natural motion during each transition. Due to limitations in our automatic segmentation algorithm, we require the user to keep the hands sufficiently far from the body, as well as from each other (for the two-hands portion of the dataset).

Segmentation. Even when properly calibrated, segmentation via simple color-space thresholding is sensitive to lighting variation, resulting in noisy annotations; see Figure 4a. Hence, we first remove small outliers by a morphological opening with a 5×5 circular kernel; see Figure 4b. We then connect nearby connected components (when elements are closer than 25 pixels), and compute the convex hull of the mask; see Figure 4c. We then retrieve the depth values of the pixels within the convex hull and compute their median. As the hull is expected to mostly contain pixels corresponding to the hand, we can identify the hand depth by computing the median of the depth pixels within the hull. We then discard any pixel with a depth sufficiently far from the mean (i.e. the radius of a sphere enclosing the hand in rest pose). Hence,

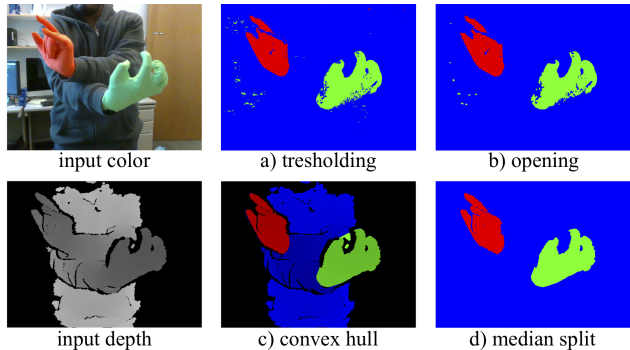


Figure 4. We combine color and depth input to extract ground truth segmentations. We first segment the color image via HSV thresholding (a), and remove noise with a morphological opening (b). The convex hull of the labels is used to extract a portion of the depth map (c). As most of the pixels within the hull correspond to the hand, the median of its depth values can be used to discard background pixels (d).

our underlying assumption is that the hands are sufficiently distant and separated from other objects in the scene. When labeling two hands the algorithm is simply executed twice, one for each label, and the results combined to generate the final mask.

5. Learning to segment hands

We now detail the structure of several learning-based semantic segmentation methods which we will then quantitatively cross-evaluate on our dataset in Section 6.

Random forests. Our first baseline is the *shallow* learning offered by Random Forests popularized for full-body tracking by Shotton et al. [32]. Tompson et al. [38] pioneered its application to binary segmentation of one hand, while Sridhar et al. [35] extended the approach to also learn more detailed part labels (e.g. palm/phalanx labels). Analogously to [32, 35], our forest consists of 3 trees each of depth 22, and uses the typical depth differential features proposed by [32, Eq.1]. At inference time, random forests are highly efficient, making them suitable to applications like real-time hand tracking. However, while their optimal parameters (offset/threshold) are learnt, the features themselves are fixed, and this can result in overall lower accuracy when compared to deep architectures; for an in-depth analysis, we refer the reader to [28].

5.1. Deep convolutional segmenters

To overcome the challenges of shallow learning, we evaluate several recently proposed deep learning convolutional architectures, as well as propose a novel variant with enhanced forward-propagation efficiency and precision; see Figure 5. As we have a multi-class labeling problem, we employ the soft-max cross entropy loss. In all our experiments

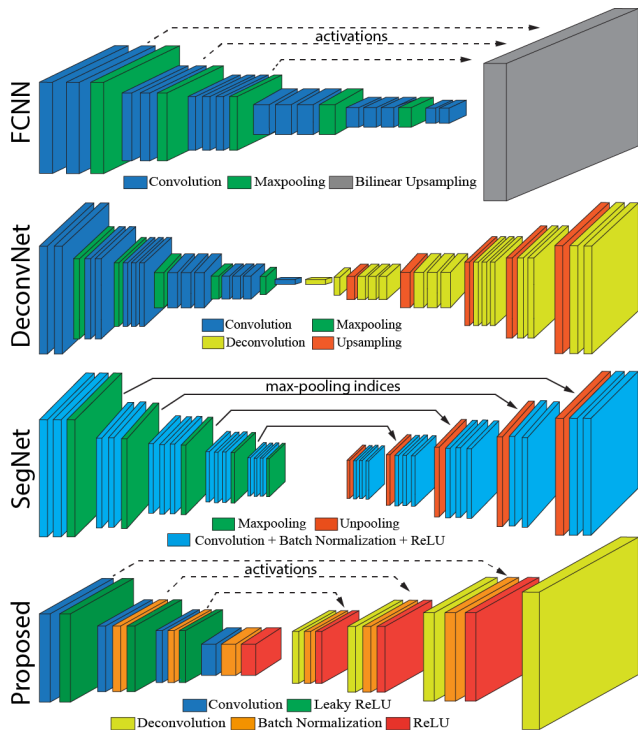


Figure 5. Semantic segmentation CNN architectures.

we train our networks with ADAM optimizer with a learning rate of 0.0002, and $\beta_1 = .5$, $\beta_2 = 0.999$ for 50 epochs on an NVIDIA Tesla P100.

Fully convolutional neural network (FCNN). Long et al. [17] proposed an architecture where a coarse segmentation mask is produced via a series of convolutions and max-pooling stages (*encoder*), where the low-resolution image is then upsampled (*decoder*) via bilinear interpolation – the *FCN32s* variant in [17, Fig.3]. As this process produces a blurry segmentation mask, a sharper mask can be obtained by combining this image with the higher-resolution activations from earlier layers in the network; the *FCN16s* and *FCN8s* variants. Unfortunately, the initial layers in the network only encode very localized features. Hence while this process does produce sharper results, it also introduces high-frequency mis-classifications in uncertain regions. Another problem of FCNN is their difficulty in dealing with the problem of *class imbalance*: in our training images, the cardinality of background pixels is significantly larger than the one of hand pixels. We overcome this problem by incorporating the class frequency in the loss [20, 40], which effectively prevents the network from converging to one that trivializes the output to be always classified as background. Even with these changes, the limited accuracy achieved by this network can be understood by noting that the encoder layer is learnt, while the decoder layer is not.

Learnt encoder-decoder networks. The popular *Seg-*

Net [1] and *DeconvNet* [22] semantic segmentation networks follow an encoder-decoder architecture. Similarly to FCNNs, the encoder is realized via a sequence of convolutions and max-pooling operations. However, rather than relying on interpolation, the decoder used to generate high-resolution segmentations is also learnt. Both architectures employ an *unpooling* operation that inverts the *max-pooling* in the encoder. Similarly to DeconvNet, SegNet upsamples the feature maps via memorized max-pooling indices in the corresponding encoder layer. Further, while unpooling in SegNet is followed by a simple series of convolutions, DeconvNet employs a series of *deconvolution* layers. This deconvolution is the *transpose* of a convolution, in turn represented by the gradient of a convolution layer. This characteristic, and the large number/size of deconvolution layers makes DeconvNet significantly more computationally intensive to train end-to-end without a justifiable increase in accuracy [1].

Proposed baseline. Our novel architecture is a *hybrid* encoder-decoder: we employ a hierarchy of deconvolution layers (a-la DeconvNet), and to improve sharpness and local detail of our predictions we forward information from encoder to decoder through skip-connections (a-la FCNN or U-Net [29]). Differently from other architectures, note how our encoders/decoders do not contain any max-pooling/unpooling layer. Pooling layers are meaningful in classification tasks, where we are interested in the maximal activation in a bank of filters without retaining fine-grained information about its spatial structure. However, the definition of a downsampling layer is essential, as a bottleneck in the network is necessary to learn the low-dimensional manifold of hand appearance. In our encoder network, this is achieved by *stride-2 convolution* layers. As pooling indices are not available, in the decoder we symmetrically employ *stride-2 deconvolution* layers, as this enables the network to learn an appropriate upsampling filter. The simplicity in our design results in efficient forward propagation, while simultaneously achieving superior accuracy; see Table 2.

6. Evaluation

We quantitatively evaluate our dataset and learning architecture from three different angles according to the metrics defined below. In Section 6.1, we evaluate the performance of several classical learning architectures on our data, revealing how our proposed architecture can produce state-of-the-art accuracy, while remaining efficient in terms of forward-propagation. In Section 6.2, we document the need for larger training datasets in this applicative domain. In Section 6.3, we train the same network on different datasets, and compare the ability of a network trained on a dataset to generalize to others.

Evaluation metrics. In our multi-label classification problem, each pixel can be classified as {left, right, background}.

	mIoU	Time		IoU			Precision			Recall		
		train	test	left	right	bg	left	right	bg	left	right	bg
FCN(32s)	78.1	36h	8ms	78.2	78.1	82.4	78.2	77.8	99.3	67.9	68.1	99.6
Forests	84.5	6h	1ms	82.5	86.4	96.1	91.9	89.1	99.5	88.2	96.2	96.4
SegNet	87.7	50h	21ms	92.1	83.4	87.3	88.7	71.5	99.8	94.6	92.2	99.3
Proposed	97.2	22h	5ms	97.6	96.9	97.9	98.2	98.7	99.9	96.8	95.1	99.9

Table 2. The performance of several learning-based segmentation methods trained on our dataset.

Within each class, we can have *true-positives* (TP), *false-positives* (FP) and *false-negatives* (FN). Given such a categorization, we can then recall the notions of *precision*, *recall* (equivalent to *accuracy* in this scenario), and *Intersection over Union* (IoU) that will use for quantitative evaluation:

$$\text{Precision} = |TP| / (|TP| + |FP|)$$

$$\text{Recall} = |TP| / (|TP| + |FN|)$$

$$\text{IoU} = |TP| / (|TP| + |FP| + |FN|)$$

To summarize results and avoid bias due to class imbalance, our mean IoU (mIoU) is the average of the IoU of the left/right class only (ignoring the background).

6.1. Segmenting with different architectures

In Table 2, we compare the different learning approaches in terms of accuracy, as well as training and test time. Although Random Forests are clearly the fastest to train and to infer on, they perform poorly when compared to deep networks. As we will discuss in Section 6.3, this is enabled by the size of our training dataset. Due to its simple up-sampling scheme, FCN(32s) performs the worst among the evaluated networks which manifests in low precision/recall scores for hands, while performing well on the background class. Thanks to its learnt decoder network, SegNet obtains much better results. However its architecture is too heavy, resulting in a runtime that is not suitable for real-time tracking applications. Our proposed architecture not only outperforms the others in terms of accuracy, but it is also fast to forward-propagate, running at ≈ 200 fps. The increase in accuracy of our network can be justified by the fact that downsampling operators are learnt, rather than max-pooled, and by the connections bringing high-frequency information into the decoder layer.

Due to slow training we were not able to perform quantitative comparison to DeconvNet (a single epoch took over 12 hours to complete). Note how DeconvNet has 15 deconvolution layers, while we only have 4. Given its architecture, we expect it to have an inference time even larger than the one we measured on SegNet. Comparatively, our network should also be easier to train, as vanishing gradients are resolved via skip-connections, while batch-normalization further helps speed-up training.

6.2. Effectiveness of large training datasets

In Table 3, we report the results of training our network on datasets of progressively larger size. This is achieved by randomly sub-sampling our dataset into smaller ones. Similarly to the observations made by Sun et al. [36], segmentation accuracy has a *quasi*-logarithmic dependency on the training set size. This can be better appreciated in Figure 6, where the IoU metrics are plotted against dataset size on a log-scale. This analysis highlights the importance of new larger datasets in this applicative domain.

6.3. Cross-dataset evaluation

We test our baseline network by training/testing on all possible combinations of the datasets in Table 1 which are summarized in Table 6.2 in terms of mIoU (see **supplemental material** for details). For comparisons where only one hand is considered, we coalesce the left/right labels to compute our metrics. Testing a network that is trained on the *same* dataset clearly provides the highest accuracy. This is expected, as not only noise and structured-outliers are sensor-specific, but there are also slight inconsistencies in the meaning of “ground-truth” across datasets (e.g. how much of the wrist is considered). Nonetheless, the very low off-diagonal entries clearly illustrate how more effort should be invested in the development of learning architectures that are sensor-invariant and suitable to transfer learning.

HandSeg and HandNet are acquired with the same sensor, and are comparable in size, yet the performance of training the network is *drastically* different (we perform $\approx 30\%$ better). This clearly reveals how relying on heuristics for ground-truth annotation can be *highly* detrimental towards the generation of high-quality datasets. We expect

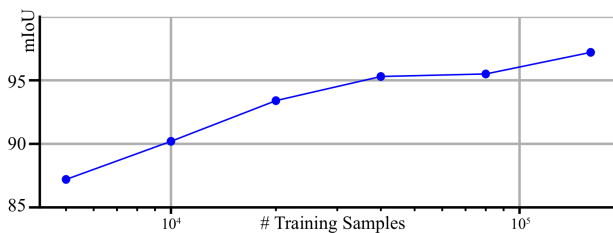


Figure 6. The unreasonable effectiveness of big data

	Summary	IoU (per-class)			Precision (per-class)			Recall (per-class)		
# Images	mIoU	left	right	bg	left	right	bg	left	right	bg
5k	87.2	87.3	87.1	93.9	86.3	90.2	99.7	85.2	81.2	99.91
10k	90.2	90.6	89.9	95.0	91.3	92.9	99.78	88.4	85.4	99.94
20k	93.4	93.8	93.1	96.0	94.7	96.1	99.82	92.2	89.6	99.96
40k	95.3	95.8	94.8	96.8	96.9	97.3	99.85	94.4	92.0	99.97
80k	95.5	96.0	95.0	96.9	96.4	98.4	99.85	95.4	91.5	99.97
160k	97.2	97.6	96.9	97.9	98.2	98.7	99.90	96.8	95.1	99.98

Table 3. Impact of training set size on hand segmentation (trained on our network).

similar conclusions could be made when employing analogous heuristics to annotate much larger datasets such as BigHand2.2M [41].

Training on neither NYU nor Freiburg performs particularly well. Note how NYU performs better than Freiburg, but this can be justified via the fact that NYU data is simpler and more self-consistent, hence requiring less variation in the training data. As Freiburg is synthetic in nature, our analysis reveals it is *too small in size* to effectively capture the targeted pose/shape complexity. The necessity of larger datasets for the effective training of deep networks is also evident by comparing our network performance to the random forest results reported by Tompson et al. [38], where they achieved a higher performance (classification error $\approx 4.1\%$).

6.4. Qualitative evaluation

In Figure 8, we provide qualitative segmentation results on our proposed dataset. As expected, the bilinear upsampling of FCNN loses many of the details, resulting in blob-like segmentation masks. By learning the decoder SegNet can perform better, but fine-grained details can still be blurred out; see sample #3 and #4. In comparison, our network can resolve fine-grained details thanks to the reuse of encoder feature maps in the decoder. Sample #6 and #7 show typical failure cases of our architecture, where a part of the left hand is mis-classified as right – these type of mistakes would create large outliers in a tracking optimization and could be avoided via regularization layers [4, 43], or by training with a loss that accounts these configurations [11]. Figure 7 shows other challenging frames. Sample #1 illus-

Test Train	NYU	HandSeg	HandNet	Freiburg
NYU	91.6	69.8	44.8	67.8
HandSeg	77.0	97.2	47.0	48.2
HandNet	50.0	53.8	66.9	48.5
Freiburg	80.3	52.0	45.5	81.2

Table 4. Generalization across datasets (mIoU).

trates how the network can still segment the hands of multiple persons, although it was trained on frames containing a single individual. This reveals the generalization capabilities of our network, which did not only learn to segment *one/two* regions, but also learnt a latent *shape-space* for human hands. Sample #2 shows a person holding a cup, while Sample #3 has the hand lying flat on the body. These scenarios are difficult, as the network has never seen a hand interacting with objects. Accuracy could be improved by accounting for the additional information in the color channel, or by learning the appearance of the object via training examples.

7. Conclusions and future works

We introduced a new high-quality dataset for hand segmentation that is significantly larger than what is currently available². Our dataset contains high-accuracy dense pixel annotations, large pose variations, and many different sub-

²at an equivalent annotation quality level, hence excluding [39]

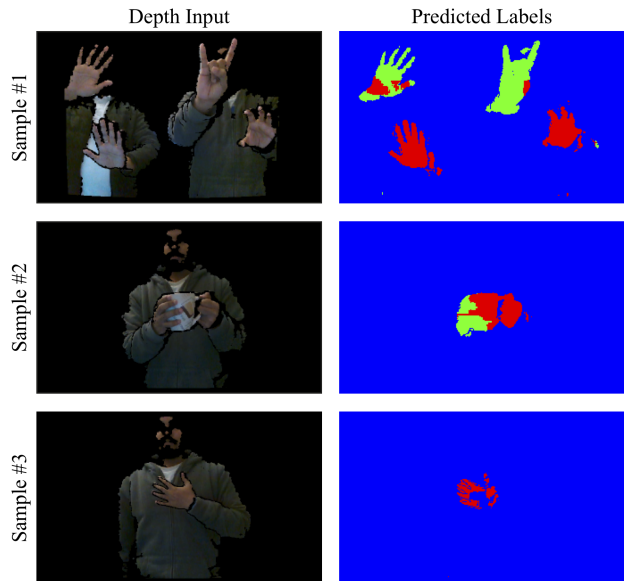


Figure 7. A selection of challenging segmentation frames.

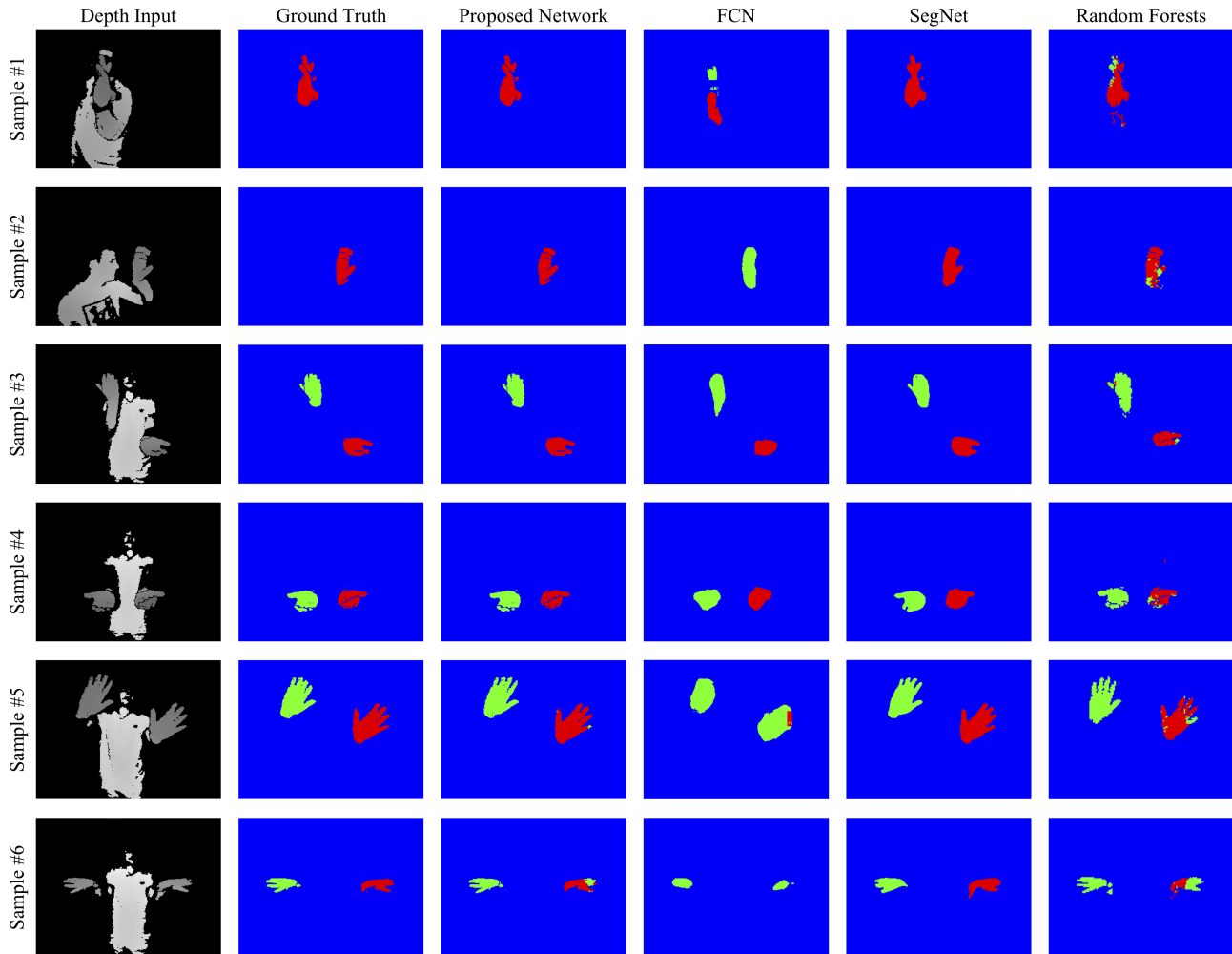


Figure 8. We illustrate a few examples of hand segmentation performance across the considered learning techniques.

jects. Our results show that larger datasets are *essential* for the development of more accurate segmentation models, and the new dataset enables effective training of deep networks for real-time hand tracking applications.

Our analysis has also revealed poor generalization characteristics for currently available methods. With the Microsoft Kinect v1 sensor being retired from production, this creates an immediate problem as the only high-quality (albeit small) dataset for the task at hand [38] becomes unusable. Conversely, our data is acquired on Intel RealSense SR300 sensors, one of the most commonly employed sensors available. Beyond these immediate needs, it would also be interesting to see whether simultaneously training on multiple datasets could generate architectures that are apt to transfer learning. While eventually the use of (very large) synthetic datasets like [45] could be very effective for training, the proposed HandSeg dataset will remain valuable for validation/testing.

We also propose a novel segmentation network that is faster than existing baselines, and provides superior mIoU

accuracy. While these results are encouraging, our dataset opens new frontiers for investigation, such as the effectiveness of spatially-aware losses [11], the use of efficient quantized networks [8], or its use for weak-supervision of discriminative hand tracking [21].

References

- [1] V. Badrinarayanan, A. Kendall, and R. Cipolla. Segnet: A deep convolutional encoder-decoder architecture for image segmentation. *arXiv preprint arXiv:1511.00561*, 2015.
- [2] S. Bambach, S. Lee, D. J. Crandall, and C. Yu. Lending a hand: Detecting hands and recognizing activities in complex egocentric interactions. In *Proc. ICCV*, 2015.
- [3] P. Buehler, M. Everingham, D. P. Huttenlocher, and A. Zisserman. Long term arm and hand tracking for continuous sign language tv broadcasts. In *Proc. BMVC*, 2008.
- [4] L.-C. Chen, G. Papandreou, I. Kokkinos, K. Murphy, and A. L. Yuille. Semantic image segmentation with deep convolutional nets and fully connected crfs. In *Proc. ICLR*, 2015.

- [5] J. R. del Solar and R. Verschae. Skin detection using neighborhood information. In *Automatic Face and Gesture Recognition*, 2004.
- [6] M. Everingham, L. Van Gool, C. K. I. Williams, J. Winn, and A. Zisserman. The PASCAL Visual Object Classes Challenge 2012 (VOC2012) Results, 2012.
- [7] K. He, G. Gkioxari, P. Dollár, and R. B. Girshick. Mask R-CNN. In *Proc. ICCV*, 2017.
- [8] I. Hubara, M. Courbariaux, D. Soudry, R. El-Yaniv, and Y. Bengio. Binarized neural networks. In *Advances in neural information processing systems*, 2016.
- [9] M. Kawulok, J. Kawulok, and J. Nalepa. Spatial-based skin detection using discriminative skin-presence features. *Pattern Recognition Letters*, 2014.
- [10] P. Kohli, J. Rihan, M. Bray, and P. H. S. Torr. Simultaneous segmentation and pose estimation of humans using dynamic graph cuts. *IJCV*, 2008.
- [11] N. Kolkin, G. Shakhnarovich, and E. Shechtman. Training deep networks to be spatially sensitive. In *Proc. ICCV*, 2017.
- [12] P. Kotschieder, S. R. Bul, H. Bischof, and M. Pelillo. Structured class-labels in random forests for semantic image labelling. In *Proc. ICCV*, 2011.
- [13] P. Krähenbühl and V. Koltun. Efficient inference in fully connected crfs with gaussian edge potentials. In *Proc. NIPS*, 2011.
- [14] Laboratory for Intelligent and Safe Automobiles, UCSD. The vision for intelligent vehicles and applications (VIVA) challenge. <http://cvrr.ucsd.edu/vivachallenge/>.
- [15] G. Lin, A. Milan, C. Shen, and I. Reid. Refinenet: Multi-path refinement networks for high-resolution semantic segmentation. In *Proc. CVPR*, 2017.
- [16] Y. Liu, J. Gall, C. Stoll, Q. Dai, H.-P. Seidel, and C. Theobalt. Markerless motion capture of multiple characters using multi-view image segmentation. *PAMI*, 2013.
- [17] J. Long, E. Shelhamer, and T. Darrell. Fully convolutional networks for semantic segmentation. In *Proc. CVPR*, 2015.
- [18] S. Melax, L. Keselman, and S. Orsten. Dynamics based 3d skeletal hand tracking. In *Proc. of GI*, 2013.
- [19] A. Mittal, A. Zisserman, and P. H. S. Torr. Hand detection using multiple proposals. In *Proc. BMVC*, 2011.
- [20] M. Mostajabi, P. Yadollahpour, and G. Shakhnarovich. Feed-forward semantic segmentation with zoom-out features. In *CVPR*, 2015.
- [21] N. Neverova, C. Wolf, F. Nebout, and G. W. Taylor. Hand pose estimation through semi-supervised and weakly-supervised learning. *Computer Vision Image Understanding*, 2017.
- [22] H. Noh, S. Hong, and B. Han. Learning deconvolution network for semantic segmentation. In *Proc. ICCV*, 2015.
- [23] M. Oberweger, P. Wohlhart, and V. Lepetit. Hands deep in deep learning for hand pose estimation. In *Proc. Computer Vision Winter Workshop*, 2015.
- [24] I. Oikonomidis, N. Kyriazis, and A. A. Argyros. Efficient model-based 3D tracking of hand articulation using kinect. In *Proc. BMVC*, 2011.
- [25] A. Paszke, A. Chaurasia, S. Kim, and E. Culurciello. Enet: A deep neural network architecture for real-time semantic segmentation. In *arXiv*, 2016.
- [26] S. L. Phung, A. Bouzerdoum Sr, and D. Chai Sr. Skin segmentation using color pixel classification: Analysis and comparison. *PAMI*, 2005.
- [27] P. O. Pinheiro, T.-Y. Lin, R. Collobert, and P. Dollr. Learning to refine object segments. In *Proc. ECCV*, 2016.
- [28] D. L. Richmond, D. Kainmueller, M. Yang, E. W. Myers, and C. Rother. Mapping stacked decision forests to deep and sparse convolutional neural networks for semantic segmentation. In *arxiv*, 2015.
- [29] O. Ronneberger, P. Fischer, and T. Brox. U-net: Convolutional networks for biomedical image segmentation. In *arXiv*, 2015.
- [30] T. Sharp, C. Keskin, D. Robertson, J. Taylor, J. Shotton, D. Kim, C. Rhemann, I. Leichter, A. Vinnikov, Y. Wei, et al. Accurate, robust, and flexible real-time hand tracking. In *Proc. of ACM CHI*, 2015.
- [31] J. Shotton, M. Johnson, and R. Cipolla. Semantic texton forests for image categorization and segmentation. In *Proc. CVPR*, 2008.
- [32] J. Shotton, A. Fitzgibbon, M. Cook, T. Sharp, M. Finocchio, R. Moore, A. Kipman, and A. Blake. Real-time human pose recognition in parts from single depth images. *CVPR*, 2011.
- [33] J. Shotton, T. Sharp, A. Kipman, A. Fitzgibbon, M. Finocchio, A. Blake, M. Cook, and R. Moore. Real-time human pose recognition in parts from single depth images. *Comm. ACM*, 2013.
- [34] S. Sridhar, A. Oulasvirta, and C. Theobalt. Interactive markerless articulated hand motion tracking using RGB and depth data. In *Proc. ICCV*, 2013.
- [35] S. Sridhar, F. Mueller, A. Oulasvirta, and C. Theobalt. Fast and robust hand tracking using detection-guided optimization. In *Proc. CVPR*, 2015.
- [36] C. Sun, A. Shrivastava, S. Singh, and A. Gupta. Revisiting unreasonable effectiveness of data in deep learning era. In *Proc. ICCV*, 2017.
- [37] A. Tagliasacchi, M. Schroeder, A. Tkach, S. Bouaziz, M. Botsch, and M. Pauly. Robust articulated-icp for real-time hand tracking. *CGF (Proc. SGP)*, 2015.
- [38] J. Tompson, M. Stein, Y. Lecun, and K. Perlin. Real-time continuous pose recovery of human hands using convolutional networks. *ACM TOG*, 2014.
- [39] A. Wetzler, R. Slossberg, and R. Kimmel. Rule of thumb: Deep derotation for improved fingertip detection. In *Proc. BMVC*, 2015.
- [40] J. Xu, A. G. Schwing, and R. Urtasun. Tell me what you see and i will show you where it is. In *CVPR*, 2014.
- [41] S. Yuan, Q. Ye, B. Stenger, S. Jain, and T.-K. Kim. Big-hand2.2m benchmark: Hand pose dataset and state of the art analysis. In *Proc. CVPR*, 2017.
- [42] H. Zhao, J. Shi, X. Qi, X. Wang, and J. Jia. Pyramid scene parsing network. In *Proc. CVPR*, 2017.
- [43] S. Zheng, S. Jayasumana, B. Romera-Paredes, V. Vineet, Z. Su, D. Du, C. Huang, and P. H. S. Torr. Conditional random fields as recurrent neural networks. In *Proc. CVPR*, 2015.
- [44] Q. Zhu, C.-T. Wu, K.-T. Cheng, and Y.-L. Wu. An adaptive skin model and its application to objectionable image filtering. In *Multimedia*, 2004.

- [45] C. Zimmermann and T. Brox. Learning to estimate 3d hand pose from single rgb images. In *Proc. ICCV*, 2017.